

Empirical rule of fruit rind fragmentation in muskmelon netting

Yuri Akiba^{1*}, Akari Ishibashi², Motohiro Sato¹, and Hiroyuki Shima^{2†}

¹Faculty of Engineering, Hokkaido University, Kita 13, Nishi 8, Kita-ku, Sapporo 060-8628, Japan

²Department of Environmental Sciences, University of Yamaguchi, 4-4-37, Takeda, Kofu, Yamaguchi 400-8510, Japan

The suberized netting tissue on the surface of muskmelons is a remnant of the rind fragmentation caused by the mechanical imbalance between the expanding flesh meat and the solidified epidermis during growth. The appearance of this netting pattern is an important indicator for assessing the quality of muskmelons; however, very few quantitative studies have been conducted on the geometry of the netting. This study statistically analyzed the areas of fine epidermis fragments surrounded by the net using image analysis and explored a common rule governing the probability distribution of the fragment area. We found that the fragment area distribution follows a universal law by the modified Bessel function, which is consistent with the theoretical argument for the fracture behavior of brittle materials.

arXiv:2006.13783v1 [physics.bio-ph] 28 Jun 2022

1. Introduction

Melon (*Cucumis melo*) is a species of cucumber (*Cucumis*) that has developed into many cultivars.¹⁾ Fresh melon meat can be either sweet or bland, with or without a musky aroma; the rind may be netted, ribbed, or smooth. Among the diverse varieties, we will focus on the sweet flesh and musky netted rind type, called muskmelons (or cantaloupe²⁾) produced in Japan. Muskmelons produced in Japan are characterized by a uniform and fine reticulate pattern that ornaments their outer surface. The reticulate pattern is an interesting topic not only in plant physiology but also in fracture mechanics.

The net of muskmelons is made of solidified secretions that have penetrated the cracks in the rind³⁾ (see fig. 1). In fact, muskmelons do not have a net in the early stage of growth; they grow to the size of chicken eggs about one week after pollination, and at this stage, the outer surfaces are still smooth with no net. Approximately two weeks after pollination, the epidermis becomes hard and enters a hardening period in which the mechanical flexibility of the epidermis is significantly reduced. During this hardening period, the growth rate of the epidermis cannot keep up with the growth rate of the meat because only the inner meat part continues to expand. As a result, many cracks begin to occur hierarchically throughout the epidermis (fig. 1(a)). Once the surface cracks, a liquid called suberin (a lipophilic polymer) is secreted from the inside, filling the gap in the cracks to prevent moisture loss (fig. 1(b)).⁴⁾ The cork-like solidified secretion in the gap is what we call the net of muskmelons (fig. 1(c)), which serves as a primary indicator for the non-destructive evaluation of muskmelons.

It was first pointed out in the early 1950s that cork-like nets that appear on the surface of Cucurbitaceae plants, including muskmelons, originate from cracks on the surface.⁵⁾ Subsequently, genetic analysis revealed the biochemical process by which suberin secreted into the gap is transformed into cork.⁶⁾ At approximately the same time, it was found that only the netted-rind type of muskmelons contained a large amount of cuticle components in the epidermis, which caused a decrease in the elasticity of the epidermis during the hardening period.⁷⁾ More recently, the structure of cell tissue involved in

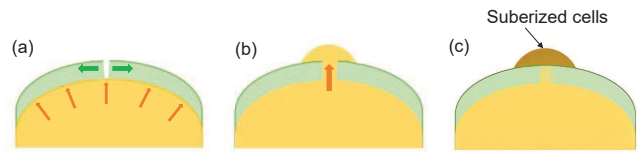


Fig. 1. Diagram of the muskmelon netting formation process (a) Swelling of fruit meat causes a local fracture of the rind. (b) Flesh cells extrude to the outside of the rind and suberin secreted from the flesh side is deposited on the extruded cell wall. (c) Suberin-deposited cell walls thicken and solidify into cork.

suberization and its biochemical properties have been elucidated by making full use of mass spectrometry and electron microscopy.⁸⁾ Nevertheless, the scope of these previous studies was limited to either the biochemical attributes or local arrangement of the cell tissue relevant to suberization. Very few examples consider the global geometry of the entire net covering the rind of muskmelons,⁹⁾ despite fundamental interest from the viewpoints of physics and engineering.

From a mechanical perspective, the rind fragmentation of muskmelons can be regarded as hierarchical fracturing of brittle shells under internal pressure-driven expansion. This fracturing process releases deformation energy driven by surface tension, often leaving a polygonal crack network, as observed in organic and inorganic systems, such as powder-water mixtures under desiccation,^{10–15)} volcanic products under cooling,^{16–19)} animal skin surfaces,²⁰⁾ and tree barks,²¹⁾ wherein volume contraction or expansion triggers the fragmentation of the material surface. In many cases, whether a particular material breaks or not depends strongly on the measurement conditions and the slight non-uniformity of the mechanical characteristics; therefore, it is not possible to draw a consistent conclusion. In contrast, global fracture patterns that spread throughout a material often follow statistical laws in terms of time or space.^{22–26)} Therefore, it can be expected that a hidden statistical law exists in the fracture pattern of muskmelon rind.

In this study, we investigated the geometry of muskmelon netting using image analysis, and scrutinized the presence of statistical laws. We calculated the areas of the rind fragments surrounded by the cork-like substance for multiple specimens

*akiyuri@eng.hokudai.ac.jp

†hshima@yamanashi.ac.jp

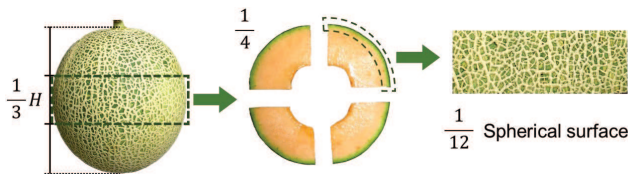


Fig. 2. Procedure of cutting a muskmelon and drawing the equatorial rind from it.

Table I. List of specimen type and dimensions.

Specimen (cultivar)	Diameter D (cm)	Height H (cm)	D/H
a (Tiara-red)	14.3	15.7	0.91
b (Tiara-red)	15.0	15.0	1.00
c (Tiara-red)	14.6	15.5	0.94
d (Lupia-red)	16.0	17.0	0.94
e (Lupia-red)	15.0	18.0	0.83

and found that the probability distribution of the fragment areas followed a universal curve. Our findings suggest the possibility of automating and objectivizing fruit selection tasks through diagnostic imaging of the rind of muskmelons.

2. Methods

2.1 Sample preparation

We used one of the well-known muskmelon cultivar called “Raiden” produced in Hokkaido, northernmost prefecture of Japan, as specimen. Two of the “Lupia-red” melons and three of the “Tiara-red” melons, both of which belong to varieties of Raiden melons, were purchased from a supermarket. The five specimens were approximately 14–16 cm in diameter, and they were often slightly vertically long (see Table I).

Each specimen was divided vertically into three equal parts (see fig. 2), and only parts around the equator were extracted. The equatorial part was further divided vertically into four parts, and only the rind was removed. For each of the cut-out rind, dark green fragments surrounded by the light green cork net were collectively photographed from the normal direction of the rind; the obtained photos were used for image analysis. We focused only on the surface of the equator, which is far from the fruit stem (top of the specimen) and flower scar (bottom). Thus, it is unnecessary to consider the effect of the presence of fruit stems and flower marks on net shape.

2.2 Image analysis

To examine the geometric area of the rind fragments and their probability distribution, the photos obtained were analyzed using an image processing software (ArcGIS, Esri).

First, the Cartesian coordinates of the actual length scale were assigned to the image data. Next, to extract the fragment areas enclosed by the net tissue from the image, the outline of the fragments was traced, and line data were created (see fig. 3(b)). The contour was specified manually because the color difference between the net (light green) and fragments (dark green) appears rather ambiguous, making it technically difficult for ArcGIS to distinguish them. Finally, the line data were converted into polygon data (fig. 3(c)) and evaluated the fragment areas. This procedure was performed on all photographs obtained from the five specimens to calcu-

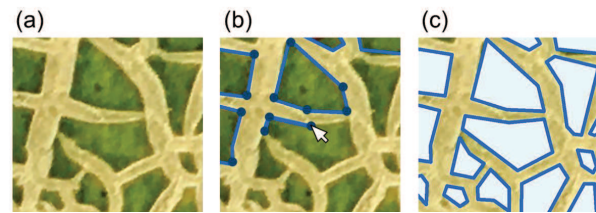


Fig. 3. Fragment area evaluation by image analysis. (a) Enlarged photograph of a muskmelon rind containing nets (light green) and fragments (dark green). (b) Contour line segments (blue lines) and vertices (black dots) were assigned along the boundary of the fragment area. (c) Polygons (light blue) identified in the fragment area.

late the frequency distribution of the fragment areas.

3. Results

3.1 Occurrence frequency of fragment area

Figure 4 shows the frequency of occurrence of fragment area s over the five different specimens listed in Table I. The five measurement datasets commonly show one wide peak slanted to the left with a fat tail at large s , while the peak position and peak height vary greatly between specimens. The total frequency of occurrence also varied from specimen to specimen, as presented in the legend. These observations indicate that the net shape of muskmelons is highly dependent on the growth conditions and exhibits large fluctuations. That is, there is no common rule for the frequency of the fragment area s itself.

In contrast to the above results, if we replace the horizontal axis from s with a normalized one, a hidden law becomes apparent. Figure 5 shows the probability distribution of the measurement data s/s_0 , where the value of s_0 was selected such that the expected value of s for each specimen was equal to unity. It is clearly seen that the probability distributions of s/s_0 derived from five different specimens show very similar curves with slight variation. This was the first main result of our study.

3.2 Two choices for fitting curve

To account for the common behavior of the probability distribution of s/s_0 , we chose two specific classes of fitting curves. The first is represented by a function of

$$P_w(s) = \frac{2k}{s_0} \left(\frac{s}{s_0}\right)^{k-1} K_0 \left[2 \left(\frac{s}{s_0}\right)^{k/2} \right], \quad (1)$$

where k is the fitting parameter and $K_0(u)$ is called the zeroth order modified Bessel function of the second kind, which monotonically decreases with u . In eq. (1), the value of s_0 is set to

$$s_0 = \left[\Gamma \left(1 + \frac{1}{k} \right) \right]^{-2}, \quad (2)$$

where $\Gamma(z) = \int_0^\infty u^{z-1} e^{-u} du$ denotes the gamma function. The setting of eq. (3) ensures that the normalization condition

$$\int_0^\infty s P_w(s) ds = 1, \quad (3)$$

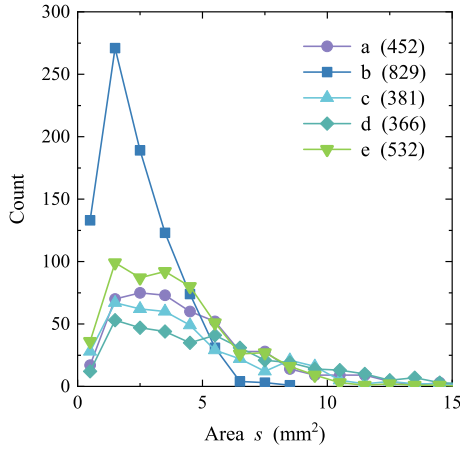


Fig. 4. Occurrence frequency of the fragment area s for five different muskmelon specimens. The legend indicates the number of fragment samples for each muskmelon specimen.

for any value of k ; see Discussion in §4.1. The other fitting curve is represented by the following:

$$P_g(s) = \frac{2}{s_0} \left(\frac{k}{\Gamma(k)} \right)^2 \left(\frac{k^2 s}{s_0} \right)^{k-1} K_0 \left(2k \sqrt{\frac{s}{s_0}} \right), \quad (4)$$

where $s_0 = 1$ is fixed, such that the normalization condition is similar to eq. (3) is satisfied. The optimized values of the fitting parameter k are generally different for $P_w(s)$ and $P_g(s)$.

Figure 5 shows the optimal fitting curves described by eqs. (1) and (4). The optimized values of k for all data points were $k = 2.4$ and $k = 3.8$ for the curves of $P_w(s)$ and $P_g(s)$, respectively. Both curves are in good agreement with the measured data. We confirmed that these fittings work well even if the data points are separated by specimens, and Table II presents the list of optimized k values when the data obtained from five individual specimens are separately fitted by eqs. (1) and (4). The fluctuations in the k value for the five specimens were within 13 % and 26 % for the P_w - and P_g -based fits, respectively. Minor fluctuations in k support the validity of our choice of fitting distribution functions for muskmelons of various sizes. The discovery of two appropriate fitting distribution functions for s/s_0 of muskmelon nets is the second main finding of this study.

4. Discussion

4.1 Derivation of K_0 -based fitting functions

The reason our experimental data of the fragment area s obey the curve represented by the distribution function $P_w(s)$ and $P_g(s)$ defined by eqs. (1) and (4), respectively, can be explained as follows:

In the field of statistical physics, it is known that^{27–29)} the size distribution of fragments produced by the fracture of brittle materials often follows a unique probability distribution function, which may belong to the Weibull or Gamma distribution. For instance, the fracture spacing in one-dimensional ring-shaped brittle materials under radial expansion was statistically analyzed;³⁰⁾ it was then proved that the probability density function of the fracture spacing in the circumferential (x) direction is approximately represented by either of the following two functions;^{31,32)} the one is Weibull distribution

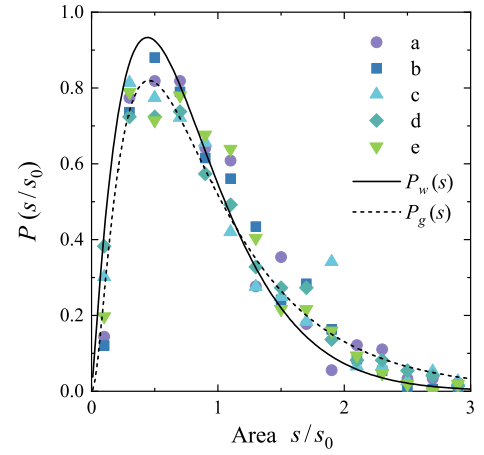


Fig. 5. Normalized probability distribution of the normalized fragment area s/s_0 . The solid and dashed curves defined by eqs. (1) and (4) are the optimized fitting curves for all data points, with settings of $k = 2.4$ and $k = 3.8$.

Table II. List of optimized fitting parameter value k .

Specimen	a	b	c	d	e	All
$P_w(s)$	2.6	2.6	2.3	2.3	2.6	2.4
$P_g(s)$	4.4	4.5	3.6	3.5	4.3	3.8

written by

$$w(x) = \frac{k}{x_0} \left(\frac{x}{x_0} \right)^{k-1} e^{-(x/x_0)^k}, \quad (5)$$

satisfying $\int_0^\infty w(x)dx = 1$, and the gamma distribution is defined as

$$g(x) = \frac{1}{x_0} \frac{k}{\Gamma(k)} \left(\frac{kx}{x_0} \right)^{k-1} e^{-kx/x_0}, \quad (6)$$

that satisfies $\int_0^\infty g(x)dx = 1$. Both distributions contain two parameters, x_0 and k , and in actual fracture phenomena, the values of the two are dependent on the material properties and experimental conditions. For each distribution, the expected value of x is expressed as

$$\langle x \rangle_w = \int_0^\infty xw(x)dx = x_0 \Gamma \left(1 + \frac{1}{k} \right), \quad (7)$$

and

$$\langle x \rangle_g = \int_0^\infty xg(x)dx = x_0. \quad (8)$$

We now hypothesize that the analysis of the fracture distribution of one-dimensional rings can be extended to explain the collapse of the expanding spherical shell segments under stretching in both the latitude (x) and longitude (y) directions. Suppose the rind of a muskmelon during growth can be regarded as an expanding spherical shell subject to internal pressure. We constantly observed a small portion of the shell until the fracture. We also assumed that the fracture spacing within the portion follows the distribution in either of eq.(5) or (6) in the x and y directions. Once one of the two is chosen, we can theoretically estimate the fragment area distribution within a portion of the shell in the following manner.

If we choose the former type of distribution w , then the

two-dimensional statistical partitioning $f(x, y)$ is given by the product of the two distributions, $f(x, y) = w(x)w(y)$, which reads

$$f(x, y) = \frac{k^2}{x_0 y_0} \left(\frac{xy}{x_0 y_0} \right)^{k-1} \exp \left[- \left(\frac{x}{x_0} \right)^k - \left(\frac{y}{y_0} \right)^k \right]. \quad (9)$$

We then transform the variables from x, y to s, q , defined as

$$s = xy, \quad q = \frac{x}{y}, \quad (10)$$

to obtain the probability density function $h(s, q)$ in terms of s, q as follows:

$$\begin{aligned} h(s, q) &= f(x(s, q), y(s, q)) \left| \frac{\partial(x, y)}{\partial(s, q)} \right| \\ &= \frac{k^2}{2(x_0 y_0)^k} \frac{s^{k-1}}{q} \exp \left[- \left(\frac{\sqrt{s q}}{x_0} \right)^k - \left(\frac{1}{y_0} \sqrt{\frac{s}{q}} \right)^k \right]. \end{aligned} \quad (11)$$

Consequently, the fragment area distribution $P_w(s)$, based on the fracture spacing $w(x)$, is given by

$$P_w(s) = \int_0^\infty h(s, q) dq. \quad (12)$$

To proceed with the calculation, we further transform the variable from q to η using the following relation:

$$q = \frac{x_0}{y_0} \exp \left(\frac{2\eta}{k} \right). \quad (13)$$

Substituting it to eq. (12), we obtain

$$\begin{aligned} P_w(s) &= \int_{-\infty}^\infty g(s, q(\eta)) \frac{dq}{d\eta} d\eta \\ &= \frac{2k}{s_0} \left(\frac{s}{s_0} \right)^{k-1} \int_0^\infty \exp \left\{ -2 \left(\frac{s}{s_0} \right)^{k/2} \cosh \eta \right\} d\eta, \end{aligned} \quad (14)$$

with $s_0 = x_0 y_0$. The integration in eq. (14) is equivalent to the integral representation of the modified Bessel function of the second kind, K_0 . Eventually, we arrive at the desired distribution function of eq. (1).

In the case of choosing another distribution, g , for the fracture spacing, parallel discussion similar to above applies; we consider the product $f(x, y) = g(x)g(y)$, which leads to the associated $h(s, q)$ and $P_g(s) = \int_0^\infty h(s, q) dq$. Through variable transformation via $q = (x_0/y_0)e^{2\eta}$, we obtain the fragment area distribution $P_g(s)$ based on the fracture spacing $g(x)$, as eq. (4).

4.2 Practical utility of fragmentation law

In practice, the quality of muskmelons is mainly evaluated by their appearance. In addition, the price difference due to the grade difference was much larger than that of the other fruits. Currently, this sorting work is performed visually by experts, such as producers and market participants. As far as the visual recognition range is concerned, muskmelons that are evaluated to be not for sale because of their low sugar content often have a non-fine netting pattern and irregular cell area distribution. However, relying on such craftsmanship can lead to arbitrary subjectivity in determining the muskmelon grades. Moreover, the number of muskmelons that can be identified manually is limited. If the relationship between the fruit growth process and the accompanying net formation pro-

cess is clarified, it is possible to obtain an index that enables automatic and objective determination of the ripening degree of the fruit by visual inspection. Such an index can be applied to the cultivation management of muskmelons.

5. Conclusion

We unveiled a hidden universal law that governs muskmelon rind fragmentation. The universal law is described by two types of probability distribution function, both of which are relevant to the modified Bessel function. The functional form of each distribution function can be derived by considering the expansion fracture of a complete spherical shell under internal pressure. These findings may open an avenue for the development of non-destructive diagnostic technology for muskmelons based on image analysis.

Acknowledgment

This work was supported by JSPS KAKENHI Grant Numbers JP21H00362, JP20J10344, JP19K03766, and JP18H03818.

- 1) H. G. Nunez-Palenius, M. Gomez-Lim, N. Ochoa-Alejo, R. Grumet, G. Lester, and D. J. Cantliffe: *Crit. Rev. Biotechnol.* **28** (2008) 13.
- 2) J. P. Fernández-Trujillo, G. E. Lester, N. Dos-Santos, J. A. Martínez, J. Esteve, J. L. Jifon, and P. Varó: *HortTechnology* **23** (2013) 266.
- 3) N. Gerchikov, A. Keren-Keiserman, R. Perl-Treves, and I. Ginzberg: *Sci. Hortic.* **117** (2008) 115.
- 4) T. Puthmee, K. Takahashi, M. Sugawara, R. Kawamata, Y. Motomura, T. Nishizawa, T. Aikawa, and W. Kumpoun: *HortScience* **48** (2013) 1463.
- 5) F. Meissner: *Österr. Bot. Z.* **99** (1952) 606.
- 6) A. Keren-Keiserman, Z. Tanami, O. Shoseyov, and I. Ginzberg: *J. Hortic. Sci. Biotechnol.* **79** (2004) 107.
- 7) A. Keren-Keiserman, Z. Tanami, O. Shoseyov, and I. Ginzberg: *Physiol. Plant.* **121** (2004) 141.
- 8) H. Cohen, Y. Dong, J. Szymanski, J. Lashbrooke, S. Meir, E. Almekias-Siegl, V. V. Zeisler-Diehl, L. Schreiber, and A. Aharoni: *Plant Physiol.* **179** (2019) 1486.
- 9) L. Li, L. Y. Chang, S. K. Ke, and D. F. Huang: *Comput. Electron. Agric.* **88** (2012) 72.
- 10) A. Nishimoto, T. Mizuguchi, and S. Kitsunezaki: *Phys. Rev. E* **76** (2007).
- 11) L. Goehring, R. Conroy, A. Akhter, W. J. Clegg, and A. F. Routh: *Soft Matter* **6** (2010) 3562.
- 12) Y. Akiba, J. Magome, H. Kobayashi, and H. Shima: *Phys. Rev. E* **96** (2017) 023003.
- 13) S. Kitsunezaki, A. Sasaki, A. Nishimoto, T. Mizuguchi, Y. Matsuo, and A. Nakahara: *Eur. Phys. J. E* **40** (2017).
- 14) Y. Akiba and H. Shima: *J. Phys. Soc. Jpn.* **88** (2019).
- 15) C. S. Tang, C. Zhu, Q. Cheng, H. Zeng, J. J. Xu, B. G. Tian, and B. Shi: *Earth Sci. Rev.* **216** (2021).
- 16) L. Goehring, L. Mahadevan, and S. W. Morris: *Proc. Natl. Acad. Sci. USA* **106** (2009) 387.
- 17) A. Lamur, Y. Lavallee, F. E. Iddon, A. J. Hornby, J. E. Kendrick, F. W. von Aulock, and F. B. Wadsworth: *Nat Commun* **9** (2018) 1432.
- 18) Y. Akiba, A. Takashima, A. Inoue, H. Ishidaira, and H. Shima: *Earth Space Sci.* **8** (2021).
- 19) Y. Akiba, A. Takashima, and H. Shima: *Phys. Rev. E* **104** (2021).
- 20) Z. Qin, N. M. Pugno, and M. J. Buehler: *Sci. Rep.* **4** (2014) 4966.
- 21) C. S. Shen, C. Zhang, X. S. Gao, and Y. L. Li: *Phil. Mag. Lett.* **100** (2020) 294.
- 22) C. A. Tang, Y. B. Zhang, Z. Z. Liang, T. Xu, L. G. Tham, P. A. Lindqvist, S. Q. Kou, and H. Y. Liu: *Phys. Rev. E* **73** (2006) 056120.
- 23) S. Ito and S. Yukawa: *Phys. Rev. E* **90** (2014) 042909.
- 24) S. Ito and S. Yukawa: *J. Phys. Soc. Jpn.* **83** (2014).
- 25) Z. Halasz, A. Nakahara, S. Kitsunezaki, and F. Kun: *Phys. Rev. E* **96** (2017) 033006.

- 26) R. Szatmari, Z. Halasz, A. Nakahara, S. Kitsunozaki, and F. Kun: *Soft Matter* **17** (2021) 10005.
- 27) C. Lu, R. Danzer, and F. D. Fischer: *Phys. Rev. E* **65** (2002) 067102.
- 28) H. A. Carmona, F. K. Wittel, F. Kun, and H. J. Herrmann: *Phys. Rev. E* **77** (2008) 051302.
- 29) A. Paluszny, X. Tang, M. Nejati, and R. W. Zimmerman: *Int. J. Solids Struct.* **80** (2016) 38.
- 30) N. F. Mott: *Proc. R. Soc. Lond. A.* **189** (1947) 300.
- 31) D. E. Grady, Applications of survival statistics to the impulsive fragmentation of ductile rings, In M. A. Meyers and L. E. Murr (eds), *Shock waves and high strain-rate phenomena in metals*, pp. 181–192. Plenum Press, London and New York, 1981.
- 32) D. E. Grady: *Int. J. Impact Eng.* **35** (2008) 1557.